Robust Phase-Space Planning for Agile Legged Locomotion over Various Terrain Topologies

Ye Zhao*, Benito Fernandez**, and Luis Sentis*
*Human Centered Robotics Laboratory, The University of Texas at Austin, USA
**Neuro-Engineering Research and Development Laboratory, The University of Texas at Austin, USA
Email: *yezhao@utexas.edu, benito@austin.utexas.edu, lsentis@austin.utexas.edu*

***Abstract*—In this study, we present a framework for phase-space planning and control of agile bipedal locomotion while robustly tracking a set of non-periodic keyframes. By using a reduced-order model, we formulate a hybrid planning framework where the center-of-mass motion is constrained to a general surface manifold. This framework also proposes phase-space bundles to characterize robustness and a robust hybrid automaton to effectively design planning algorithms. A newly defined phase-space locomotion manifold is used as a Riemannian metric to measure the distance between the disturbed state and the planned manifold. Based on this metric, a dynamic programming based hybrid controller is introduced to produce robust locomotions. The robustness of the proposed framework is validated by using simulations of rough terrain locomotion recovery from external disturbances. Additionally, the agility of this framework is demonstrated by using simulations of the dynamic locomotion over random rough terrains.**

***Index Terms*—Phase-space planning, Rough terrain locomotion, Non-periodic keyframes, Robust hybrid automaton, Dynamic programming.**

I. Introduction

Humanoid and legged robots may soon nimbly maneuver over highly rough and unstructured terrains. This study formulates a new framework for the trajectory generation and an optimal controller to achieve locomotion in those types of terrains using phase-space formalism. From prismatic inverted pendulum dynamics [1] and a desired path plan, we present a phase-space planner that can negotiate the challenging terrains. The resulting trajectories are formulated as phase-space manifolds. Borrowing from sliding mode control theory, we use the newly defined manifolds and a Riemannian metric to measure deviations due to external disturbances or model uncertainties. A control strategy based on dynamic programming is proposed, which steers the locomotion process towards the planned trajectories.

Dynamic legged locomotion has been a center of attention for the past few decades [2, 3, 4, 5, 6, 7]. The work in [8] pioneered robust hopping locomotion of point-foot monoped and bipedal robots using simple dynamical models but with limited applicability to semi-periodic hopping motions. The work in [9] achieved biped point foot walking using virtual model control but is limited to planarized robots. Unassisted biped point foot locomotion in moderately rough terrains has been recently achieved by [10] and [11] using Poincaré maps [12]. However, Poincaré maps cannot be leveraged to non-periodic trajectories for highly irregular terrains. The work [13] devised switching controllers for aperiodic walking of planarized robots over flat terrains via re-defining the notion of walking stability. In contrast, our work focuses on non-periodic gaits for unsupported robots in random rough terrains.

The Capture Point method [14] provides one of the most practical frameworks for locomotion. Sharing similar core ideas, the divergent component of motion [15] and the extrapolated center-of-mass [16] were independently proposed. Extensions of the Capture Point method [17, 18], allow locomotion over rough terrains. Recently, the work in [19] generalizes the Capture Point method by proposing a "Nonlinear Inverted Pendulum" model, but it is limited to the two-dimensional case, and angular momentum control is ignored. The main difference from the above studies is that our controller provides a robust optimal recovery strategy and ensures stability to achieve under-actuated dynamic walking over rough terrains.

Optimal control for legged locomotion over rough terrains is explored in [20, 21, 22, 23, 24]. The work in [25] proposed an effective control technique to stabilize non-periodic motions of under-actuated robots, with a focus on walking over uneven terrain. The controller is formulated by constructing a lower-dimensional system of coordinates transverse to the target cycle and then computing a receding-horizon optimal controller to exponentially stabilize the linearized dynamics of the transverse states. Recently, a follow-up to this research enables the generations of non-periodic locomotion trajectories [26]. In contrast with these works, we propose a robust metric based optimal controller to recover from disturbances. Additionally, our framework enables maneuvers in different types of terrains, such as walking on acute slopes.

Numerous studies have focused on recovery strategies upon disturbances [27, 28]. Various recovery methods are proposed: ankle, hip, and stepping strategies [29]. In [30], a stepping controller triggered by ground contact forces is implemented in a humanoid robot. The study in [31] considers a counteracting hip angular momentum for planar biped locomotion. In our study, we concentrate on torso angular momentum and stepping strategies. Additionally, we control the center-of-mass (CoM) apex height to modulate the ground reaction force.

Phase space techniques are analogous to kino-dynamic planning [32]. However, a drawback of kino-dynamic planning is its inability to incorporate feedback control policies and robustness metrics. Our study proposes dynamic programming to achieve robust control performance. Computational

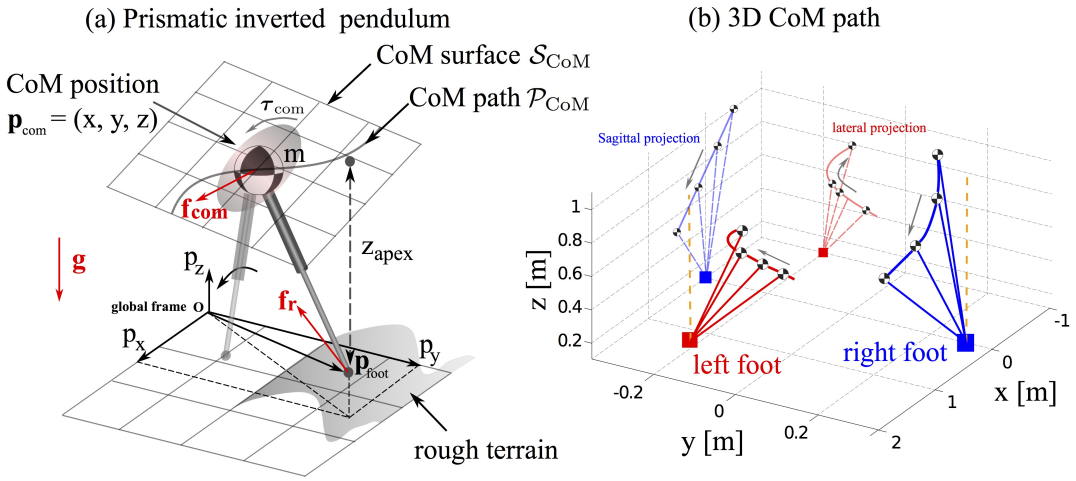

Fig. 1: 3D prismatic inverted pendulum model. (a) We define a prismatic inverted pendulum model with all of its mass located at its base while equipping it with a flywheel to generate moments. We restrict the movement of the center-of-mass to 3D planes $\mathcal{S}_{\text{CoM}}$. (b) shows motions of pendulum dynamics restricted to a 3D plane.

tractability is one of our targets. Our strategy is to design optimal controllers in the phase-space of the robot center-of-mass, which can characterize key locomotion states.

In light of the discussions above, our contributions are summarized as follows: (1) we synthesize motion plans in the phase-space to maneuver over irregular terrains, (2) a phase-space manifold is formulated and used as a Riemannian metric to measure trajectory deviations and create an in-step controller, and (3) we derive a hybrid optimal controller to recover from disturbances and study its stability.

II. Prismatic Inverted Pendulum Dynamics on a Parametric Surface

The dynamics of point foot bipedal robots in generic terrain topologies during single contact can be mechanically approximated as an inverted pendulum model [33] (see Fig. 1). We propose a prismatic inverted pendulum model (PIPM) [1] with a flywheel, and all of its mass is concentrated on the hip position (defined as the 3D CoM position, $\boldsymbol{p}_{\text{com}} = (x, y, z)^T$ with flywheel orientation angles $\boldsymbol{R} = (\phi, \theta, \psi)^T$). Since the objective of the locomotion process is to move the robot's CoM along a certain path from point A to B over a terrain, we first specify a 3D surface, $\mathcal{S}_{\text{CoM}}$, where the CoM path exists via the implicit form,

$$\mathcal{S}_{\text{CoM}} = \Big\{ \boldsymbol{p}_{\text{com}} \in \mathbb{R}^3 \mid \psi_{\text{CoM}}(\boldsymbol{p}_{\text{com}}) = 0 \Big\}. \quad (1)$$

This surface can be specified in various ways, such as via piecewise arc geometries [34, 35]. Once the controller is designed, the CoM will follow a concrete path $\mathcal{P}_{\text{CoM}}$ (as shown in Fig. 1), which we specify via piecewise splines described by a progression variable, $\zeta \in [\zeta_{j-1}, \zeta_j]$, for the j^{th} path manifold, i.e.

$$\mathcal{P}_{\text{CoM}} = \bigcup\nolimits_j \mathcal{P}_{\text{CoM}_j} \subseteq \mathcal{S}_{\text{CoM}},$$

where $\mathcal{P}_{\text{CoM}_j} = \Big\{ \boldsymbol{p}_{\text{com}_j} \in \mathbb{R}^3 \mid \boldsymbol{p}_{\text{com}_j} = \sum_{k=0}^{n_p} \boldsymbol{a}_{jk} \zeta^k \Big\}$, and n_p is the order of the spline degree. The progression variable ζ is therefore the arc length along the CoM path acting as the Riemannian metric for distance. Each $\boldsymbol{a}_{jk} \in \mathbb{R}^3$ is the coefficient vector for the k^{th} order. To guarantee the spline smoothness, $\boldsymbol{p}_{\text{com}}$ requires the connection points, i.e., the knots at progression instant ζ_j, to be $\mathcal{C}^{n_p-1}$ continuous,

$$\boldsymbol{p}^{[l]}_{\text{com}_j}(\zeta_j) = \frac{d^l \boldsymbol{p}_{\text{com}_j}}{d\zeta^l}(\zeta_j) = \boldsymbol{p}^{[l]}_{\text{com}_{j+1}}(\zeta_j), \ \forall\, 0 \le l \le n_p - 1$$

The purpose of introducing the CoM manifold $\mathcal{S}_{\text{CoM}}$ is to constrain CoM motions on the surfaces that are designed to conform to generic terrains while allowing free motions within this surface. Tracking a concrete path is achieved by selecting proper control inputs, which will be described in Section IV. The CoM path manifold, $\mathcal{P}_{\text{CoM}}$ (embedded in $\mathcal{S}_{\text{CoM}}$), can be represented in the phase-space $\boldsymbol{\xi}$. We name this representation the *phase-space manifold* and define it as,

$$\mathcal{M}_{\text{CoM}_j} = \Big\{ \boldsymbol{\xi} \in \mathbb{R}^6 \mid \sigma_j(\boldsymbol{\xi}) = 0 \Big\}, \quad (2)$$

with $\mathcal{M}_{\text{CoM}} = \bigcup_j \mathcal{M}_{\text{CoM}_j}$, which is the key manifold used in our phase-space planning and control framework. The function $\sigma_j(\boldsymbol{\xi})$ is a measure of the Riemannian distance to the nominal phase-space manifold.

A. Dynamic Equations of Motion

The pendulum dynamics can be formulated via dynamic balance of moments of the pendulum system. For our single contact scenario, the sum of moments, $\mathbf{m}_i$, with respect to the global reference frame (see Fig. 1) is

$$\sum_i \mathbf{m}_i = -\boldsymbol{p}_{\text{foot}} \times \boldsymbol{f}_r + \boldsymbol{p}_{\text{com}} \times \Big(\boldsymbol{f}_{\text{com}} + m\,\boldsymbol{g} \Big) + \boldsymbol{\tau}_{\text{com}} = 0,$$

where, $\boldsymbol{p}_{\text{foot}} = (x_{\text{foot}}, y_{\text{foot}}, z_{\text{foot}})^T$ is the position of the foot contact point, $\boldsymbol{f}_r$ is the three-dimensional vector of ground reaction forces, $\boldsymbol{f}_{\text{com}} = m(\ddot{x}, \ddot{y}, \ddot{z})^T$ is the vector of center-of-mass inertial forces, $\boldsymbol{\tau}_{\text{com}} = (\tau_x, \tau_y, \tau_z)^T$ is the vector of angular moments of the modeled flywheel attached to the inverted pendulum, m is the total mass, and $\boldsymbol{g} \in \mathbb{R}^3$

corresponds to the gravity field. The linear force equilibrium can be formulated as $\boldsymbol{f}_r = \boldsymbol{f}_{\text{com}} + m\,\boldsymbol{g}$, allowing us to simplify the equation above to:

$$\Big(\boldsymbol{p}_{\text{com}} - \boldsymbol{p}_{\text{foot}}\Big) \times (\boldsymbol{f}_{\text{com}} + m\,\boldsymbol{g}) = -\boldsymbol{\tau}_{\text{com}}. \tag{3}$$

For our purposes, we focus on the class of PIPM dynamics whose center-of-mass is restricted to a path surface $\mathcal{S}_{\text{CoM}}$ as indicated in Eq. (1). Moreover, for simplicity we only consider 3D piecewise linear surfaces. Considering as our output state the CoM positions, $\boldsymbol{p}_{\text{com}}$, the state space, $\boldsymbol{\xi} = (\boldsymbol{p}_{\text{com}}^T, \dot{\boldsymbol{p}}_{\text{com}}^T)^T = (x, y, z, \dot{x}, \dot{y}, \dot{z})^T \in \Xi \subseteq \mathbb{R}^6$ is the phase-space vector. From Eq. (3) it can be shown that the PIPM dynamics for a walking step, indexed by a discrete variable q, are simplified to the control system

$$\dot{\boldsymbol{\xi}} = \boldsymbol{\mathcal{F}}(q, \boldsymbol{\xi}, \boldsymbol{u}) = \begin{pmatrix} \dot{x} \\ \dot{y} \\ \dot{z} \\ \underbrace{\omega_q^2(x - x_{\text{foot}_q}) - \dfrac{\omega_q^2}{mg}(\tau_y + b_q\tau_z)}_{A} \\ \underbrace{\omega_q^2(y - y_{\text{foot}_q}) - \dfrac{\omega_q^2}{mg}(\tau_x + a_q\tau_z)}_{B} \\ a_q A + b_q B \end{pmatrix}, \tag{4}$$

where the phase-space asymptotic slope is defined as

$$\omega_q = \sqrt{\frac{g}{z_{\text{apex}_q}}}, \tag{5}$$

$z_{\text{apex}_q} = (a_q x_{\text{foot}_q} + b_q y_{\text{foot}_q} + c_q - z_{\text{foot}_q})$, a_q and b_q are the slope coefficients while c_q is the constant coefficient for the linear CoM path surfaces that we consider, i.e. $\psi_{\text{CoM}_q}(x, y, z) = z - a_q x - b_q y - c_q = 0$. We have defined z_{apex_q} such that it corresponds to the vertical distance between the CoM and the location of the foot contact at the instant when the CoM is on the top of the foot location. $\boldsymbol{\mathcal{F}}$ represents a vector field of inverted pendulum dynamics. In general, there is an input control policy, $\boldsymbol{u} = \boldsymbol{\pi}(q, \boldsymbol{\xi})$, where we define a hybrid control vector for our control system as $\boldsymbol{u} = \{\omega_q, \boldsymbol{\tau}_{\text{com}_q}, \boldsymbol{p}_{\text{foot}_q}\} \in \mathcal{U}$, where, $\mathcal{U}$ is an open set of admissible control values.

Remark 1. *Previously we observed that the CoM of human walking approximately follows the slope of a terrain [1, 36]. Based on this observation, we, (i) design piecewise linear CoM planes in parallel with terrain slopes; (ii) adjust the CoM planes to approximate the ballistic trajectories observed in human walking.*

Remark 2. *After producing the previous piecewise linear CoM planes, we generate phase-space trajectories by using the PIPM dynamics in Eq. (4), and smoothen the phase-space transitions through a multi-contact process. To that end, we fit a fifth-order polynomial to the multi-contact phase of each step [1]. Additionally, to further guarantee the smoothness of the contact forces during step transitions, we control the internal forces between the contact feet. We will show the smooth CoM accelerations and leg forces in the simulation section. A similar multi-contact transition strategy, named as "Continuous Double Support" trajectory generator, is proposed in [37] to achieve smooth leg force profiles.*

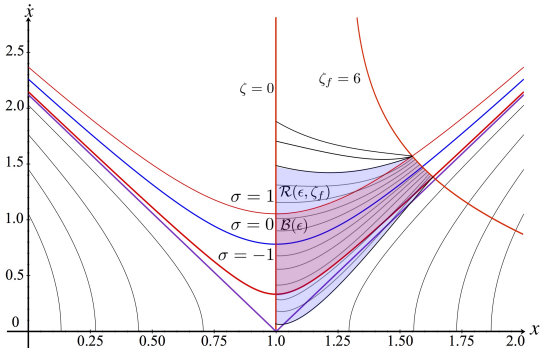

Fig. 2: Phase-space invariant and recoverability bundles. This figure shows the invariant bundle, $\mathcal{B}(\epsilon)$ (shown in red) and the recoverability bundle, $\mathcal{R}(\epsilon, \zeta_f)$ (shown in blue) in Cartesian space. If the condition when we expect the transition to occur is at $\zeta = \zeta_f$, the recoverability bundle shows the range of perturbations that can be tolerated at different ζ – the system recovers to the invariant bundle before ζ_f.

III. Hybrid Phase-Space Planning

In this section we devise a robust hybrid automaton [38, 39] with the following key features: i) an invariant bundle and a recoverability bundle to characterize robustness, and ii) a non-periodic step transition strategy. The hybrid automaton governs the planning process across multiple walking steps and as such constitutes the theoretical core of our proposed locomotion planning framework.

A. Phase-Space Bundles

Let us focus on sagittal plane dynamics first. For practical purposes we will use the symbol $\boldsymbol{x} = \{x, \dot{x}\}$ to describe the sagittal CoM state space. Eq. (2) can thus be re-considered in the output space as $\mathcal{M}_{\text{CoM}_q} = \big\{\boldsymbol{x} \in \mathcal{X} \;\big|\; \sigma_q(\boldsymbol{x}) = 0\big\}$, where σ_q is the normal distance deviated from the manifold $\mathcal{M}_{\text{CoM}_q}$.

Definition 1 (Invariant Bundle)**.** *A set $\mathcal{B}_q(\epsilon)$ is an invariant bundle if, given $\boldsymbol{x}_{\zeta_0} \in \mathcal{B}_q(\epsilon)$, with $\zeta_0 \in \mathbb{R}_{\geq 0}$, and an increment $\epsilon > 0$, $\boldsymbol{x}_\zeta$ stays within an ϵ-bounded region of $\mathcal{M}_{\text{CoM}_q}$,*

$$\mathcal{B}_q(\epsilon) = \Big\{\boldsymbol{x} \in \mathcal{X} \;\Big|\; |\sigma_q(\boldsymbol{x})| \leq \epsilon\Big\},$$

where, ζ_0 and ζ are initial and current phase progression variables, respectively. $\boldsymbol{x}_{\zeta_0}$ is an initial condition.

This type of bundle characterizes "robust subspaces" ("tubes") around nominal phase-space trajectories which guarantee that, if the state initializes within this space, it will remain on it.

Definition 2 (Finite-Phase Recoverability Bundle)**.** *The invariant bundle $\mathcal{B}_q(\epsilon)$ around a phase-space manifold $\mathcal{M}_{\text{CoM}_q}$ has a finite-phase recoverability bundle, $\mathcal{R}_q(\epsilon, \zeta_f) \subseteq \mathcal{X}$ defined as,*

$$\mathcal{R}_q(\epsilon, \zeta_f) = \Big\{\boldsymbol{x}_\zeta \in \mathcal{X}, \zeta_0 \leq \zeta \leq \zeta_f \;\Big|\; \boldsymbol{x}_{\zeta_f} \in \mathcal{B}_q(\epsilon)\Big\}.$$

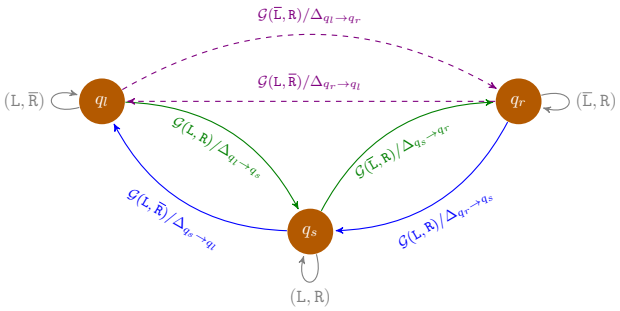

Fig. 3: This figure shows the hybrid locomotion automaton for a biped walking process. This automaton has three generic discrete modes $\mathcal{Q} = \{q_l, q_s, q_r\}$, that represent when the robot is in left leg contact (q_l), in right leg contact (q_r), and in dual stance contact (q_s), respectively. The guard $\mathcal{G}(q_k, q_{k+1})$ and the transition map $\Delta_{q_k\to q_{k+1}}$ are shown along the mode transition lines. This locomotion automaton has non-periodic mode transitions.

(a) step transition with multi-contact phase (b) step transition with invariant bundle

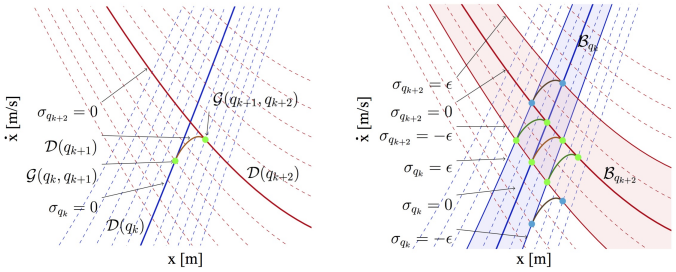

Fig. 4: Step transitions. This figure illustrates two types of step transitions in the sagittal phase-space, associated with σ-isolines. (a) switches between two single contacts with a multi-contact phase. (b) shows several guard alternatives for multi-contact transitions, from the current single-contact manifold value σ_{q_k} to the next single-contact manifold $\sigma_{q_{k+2}}$. In particular, the invariant bundle bounds, $\sigma_{q_k} = \pm\epsilon$ are shown. The transition phase in green reattaches to the nominal manifold, $\sigma_{q_{k+2}} = 0$, while the transition phase in brown maintains its σ value, i.e., $\sigma_{q_{k+2}} = \sigma_{q_k}$.

Note that this bundle assumes the existence of a control policy for recoverability. We will later use these metrics to characterize robustness of our controllers. Visualization of invariant and recoverability bundles are shown in Fig. 2.

B. Hybrid Locomotion Automaton

Legged locomotion is a naturally hybrid control process, with both continuous and discrete dynamics. The set $\mathcal{Q} = \{q_0, q_1, \ldots, q_k\}$ is a sequence of discrete states. Each discrete state q chooses a mode from $\{q_l, q_r, q_d\}$ representing discrete states where the support is left foot (q_l) or right foot (q_r) or dual feet (q_d) as shown in Fig. 3. On each mode, indexed by q, the continuous dynamics are represented as $\boldsymbol{\mathcal{F}}$ in Eq. (4) over a domain $\mathcal{D}(q)$. If we represent the hybrid system as a directed graph $(\mathcal{Q}, \mathcal{E})$, the nodes are represented by $q \in \mathcal{Q}$ and the edges are tuples of states $\mathcal{E}(q_k, q_{k+1})$, and $q_k, q_{k+1} \in \mathcal{Q}$, that represent the transitions between the nodes $q_k \to q_{k+1}$. The condition that triggers the event (switching or jump) is determined by a guard $\mathcal{G}(q_k, q_{k+1})$ for the particular edge $\mathcal{E}(q_k, q_{k+1})$.[1] We now formulate a robust hybrid automaton for our locomotion planner.

Definition 3. *A phase-space robust hybrid automaton (PSRHA) is a dynamical system, described by a n-tuple*

$$\text{PSRHA} := (\zeta, \mathcal{Q}, \mathcal{X}, \mathcal{U}, \mathcal{W}, \mathcal{F}, \mathcal{I}, \mathcal{D}, \mathcal{R}, \mathcal{B}, \mathcal{E}, \mathcal{G}, \Delta), \quad (6)$$

where ζ is the phase-space progression variable, $\mathcal{Q}$ is the set of discrete states, $\mathcal{X}$ is the set of continuous states, $\mathcal{U}$ is the set of control inputs, $\mathcal{W}$ is the set of disturbances, $\mathcal{F}$ is the vector field, $\mathcal{I}$ is the initial condition, $\mathcal{D}$ is the domain, $\mathcal{B}$ and $\mathcal{R}$ are the invariant and recoverability bundles, respectively, and will be used in the next section to design robust controllers. $\mathcal{E} := \mathcal{Q} \times \mathcal{Q}$ is the edge, $\mathcal{G} : \mathcal{Q} \times \mathcal{Q} \to 2^{\mathcal{X}}$ is the guard, and Δ is the transition map. More detailed definitions of Δ can be found in [39].

A directed diagram of this non-periodic automaton is shown in Fig. 3. To demonstrate the usefulness of this hybrid automaton, we provide an example of a planning process as follows.

[1]More definitions for various detailed transitions are in [38].

Example 1. *Consider a phase-space trajectory fragment that contains two consecutive walking steps $\mathcal{Q} = \{q_k, q_{k+1}\}$ (e.g., left and right feet). Given an initial condition $(\zeta_0, q_k, \boldsymbol{x}_{q_k}(\zeta_0)) \in \mathcal{I}$, the system will evolve following the differential dynamical system $\boldsymbol{\mathcal{F}}_{q_k}$ as long as $\boldsymbol{x}_{q_k}$ remains in $\mathcal{D}(q_k)$ (left foot on the ground, right foot swinging). If at some moment $\boldsymbol{x}_{q_k}$ reaches the guard $\mathcal{G}(q_k, q_{k+1})$ (right foot touches the ground) of some edge $\mathcal{E}(q_k, q_{k+1})$, the discrete state switches to q_{k+1}. At the same time, the continuous state gets reset to some value by $\Delta_{q_k\to q_{k+1}}$ (left and right feet switch). After this discrete transition, continuous evolution resumes and the whole process repeats.*

C. Step Transition Strategy

Step transitions can be characterized as an instantaneous contact or a short multi-contact phase (Fig. 4(a)). We first create a strategy for the instantaneous contact switch, and then extend it to the multi-contact case. To characterize the non-periodic mapping associated with the walking in rough terrains, we define a return map between keyframe states.

Definition 4 (Return Map of Non-Periodic Gaits)**.** *We define a return map of non-periodic locomotion gaits as the progression map, Φ, that takes the robot's center-of-mass from one desired keyframe state, $(\dot{x}_{\text{apex},q_k}, z_{\text{apex},q_k}, \theta_{q_k})$, to the next one, and via the control input $\boldsymbol{u}_{\boldsymbol{x}}$, i.e.,*

$$(\dot{x}_{\text{apex},q_{k+1}}, z_{\text{apex},q_{k+1}}, \theta_{q_{k+1}}) = \Phi(\dot{x}_{\text{apex},q_k}, z_{\text{apex},q_k}, \theta_{q_k}, \boldsymbol{u}_{\boldsymbol{x}}),$$

where θ_{q_k} represents the heading of the q_k^{th} walking step.

Users can design "non-periodic" keyframes to change the speed or steer the direction of the robot. For this study, we use heuristics to design keyframes. More recently, we have proposed to use a keyframe decision maker based on temporal logic [40, 41].

Definition 5 (Phase Progression Transition Value)**.** *A phase progression transition value $\zeta_{\text{trans}} : \mathcal{Q} \times \mathcal{X} \to \mathbb{R}_{\geq 0}$ is the value of the phase progression variable when the state $\boldsymbol{x}_q$ intersects a guard $\mathcal{G}$, i.e.,*

$$\zeta_{\text{trans}} := \inf\{\zeta > 0 \mid \boldsymbol{x}_q \in \mathcal{G}\}.$$

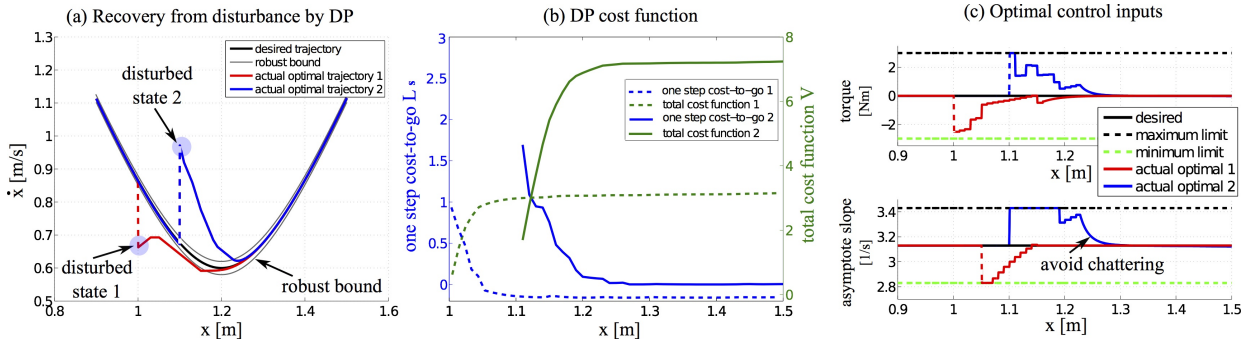

Fig. 5: Chattering-free recoveries from disturbance by the proposed optimal recovery continuous control law. Subfigure (a) show two random disturbances with positive and negative impulses, respectively. Control variables are piecewise constant within one stage as shown in subfigure (c). Simulation parameters are shown in Table I.

We propose an algorithm to find transitions between adjacent steps, which occur at ζ_{trans}. Given known step locations and apex conditions, phase-space trajectories can be obtained by the analytical solution described in the Proposition above. The phase-space trajectories of pendulum systems have infinite slopes when crossing the zero-velocity axis [42, 43]. Therefore we fit non-uniform rational B-splines (NURBS)[2] to the generated data. Subsequently, finding step transitions just consists on finding the root difference between adjacent NURBSs.

D. Phase-space Manifold

Now let us focus on proposing an analytical phase-space manifolds (PSM) and using it as a metric to measure deviations from the planned trajectories.

Proposition (Phase-Space Manifold)**.** *Given the sagittal PIPM dynamics in Eq. (4) with an initial condition* $(x_0, \dot{x}_0)$ *and foot placement* x_{foot}*, the phase-space manifold is*

$$\sigma := (x_0 - x_{\text{foot}})^2\big(2\dot{x}_0^2 - \dot{x}^2 + \omega^2(x - x_0)(x + x_0 - 2x_{\text{foot}})\big) - \dot{x}_0^2(x - x_{\text{foot}})^2 + \dot{x}_0^2(\dot{x}^2 - \dot{x}_0^2)/\omega^2, \quad (7)$$

where the condition $\sigma = 0$ *is equivalent to the nominal phase-space manifold, representing the nominal sagittal phase-space dynamics. Furthermore,* σ *represents the Riemannian distance to the nominal phase-space trajectories.*

Proof: In the nominal control case, $\tau_y = 0$. The sagittal dynamics are therefore simplied to $\ddot{x} = \omega^2(x - x_{\text{foot}})$. Since the foot placement x_{foot} is constant over the step, then $\ddot{x}_{\text{foot}} = \dot{x}_{\text{foot}} = 0$. Therefore the previous equation is equivalent to $\ddot{x} - \ddot{x}_{\text{foot}} = \omega^2(x - x_{\text{foot}})$. Defining a transformation $\tilde{x} = x - x_{\text{foot}}$, we can write $\ddot{\tilde{x}} = \omega^2\tilde{x}$. Using Laplace transformations, we have $s^2\tilde{x}(s) - \tilde{x}_0 - s\dot{\tilde{x}}_0 = \omega^2\tilde{x}(s)$. Based on this, we get

$$\tilde{x}(t) = \mathscr{L}^{-1}\{\frac{\tilde{x}_0 + s\dot{\tilde{x}}_0}{s^2 - \omega^2}\}. \quad (8)$$

By this equation, we can derive an analytical solution

$$\tilde{x}(t) = \frac{\tilde{x}_0(e^{\omega t} + e^{-\omega t})}{2} + \frac{\dot{\tilde{x}}_0(e^{\omega t} - e^{-\omega t})}{2\omega} = \tilde{x}_0\cosh(\omega t) + \frac{1}{\omega}\dot{\tilde{x}}_0\sinh(\omega t), \quad (9)$$

[2]Different from polynomials, non-rational splines or Bézier curves, NURBS can be used to precisely represent conics and circular arcs by adding weights to control points.

and by taking its derivative, we get

$$\dot{\tilde{x}}(t) = \omega\tilde{x}_0\sinh(\omega t) + \dot{\tilde{x}}_0\cosh(\omega t). \quad (10)$$

These two equations can be further expressed as

$$\begin{pmatrix} x(t) - x_{\text{foot}} \\ \dot{x}(t) \end{pmatrix} = \begin{pmatrix} x_0 - x_{\text{foot}} & \dot{x}_0/\omega \\ \dot{x}_0 & \omega(x_0 - x_{\text{foot}}) \end{pmatrix} \begin{pmatrix} \cosh(\omega t) \\ \sinh(\omega t) \end{pmatrix}$$

By using $\cosh^2(x) - \sinh^2(x) = 1$, we get

$$\big(\omega(x_0 - x_{\text{foot}})(x - x_{\text{foot}}) - \dot{x}_0\dot{x}/\omega\big)^2 - \big(-\dot{x}_0(x - x_{\text{foot}}) + \dot{x}(x_0 - x_{\text{foot}})\big)^2 = \big(\omega(x_0 - x_{\text{foot}})^2 - \dot{x}_0^2/\omega\big)^2. \quad (11)$$

After expanding the square terms and moving all terms to one side, we obtain the phase-space tangent manifold σ defined in the Proposition. ■

If we use the apex conditions as initial values, i.e. $(x_0, \dot{x}_0) = (x_{\text{foot}}, \dot{x}_{\text{apex}})$, the manifold becomes

$$\sigma = \frac{\dot{x}_{\text{apex}}^2}{\omega^2}\big(\dot{x}^2 - \dot{x}_{\text{apex}}^2 - \omega^2(x - x_{\text{foot}})^2\big). \quad (12)$$

We note that this manifold constitutes the target phase-space trajectory that we enforce the CoM to follow. This manifold implies $\tau_y = 0$. We account for changes of τ_y in the optimal controller defined in the next section to recover from disturbances. The same type of manifolds can be devised for the lateral trajectory using the pendulum dynamics in Eq. (4).

IV. Robust Hybrid Control Strategy

This section formulates a two-stage control procedure to recover from disturbances. When a disturbance occurs, the robot's CoM deviates from the planned phase-space manifolds. Various control policies can be used for the recovery. We use dynamic programming to find an optimal policy of the continuous control variables for recovery, and, when necessary, feet placements are re-planned from their initial locations. Our proposed controller relies on the distance metric of Eq. (12) to steer the robot current's trajectory to the planned manifolds.

A. First Stage: Dynamic Programming based Control

This subsection formulates the proposed dynamic programming based controller for the continuous control of the sagittal dynamics. A similar controller can be formulated for the lateral and vertical CoM behaviors, given the PIPM dynamics of

TABLE I: Dynamic Programming Parameters

Parameter	Value	Parameter	Value	Parameter	Value
nominal torque τ_y^{ref}	0 Nm	nominal asymptote slope ω^{ref}	3.13 1/s	torque range τ_y^{range}	[-3, 3] Nm
asymptote slope range ω^{range}	[2.83, 3.43] 1/s	foot placement x_{foot}	1.2 m	stage range	[0.9, 1.5] m
state range	[0.03, 1.5] m/s	stage resolution	0.01 m	state resolution	0.01 m/s
disturbed initial state s_{initial}	(1.1 m ,0.7 m/s)	desired apex velocity $\dot{x}_{\text{apex}}$	0.6 m/s	weighting scalar Γ_1	5
weighting scalar Γ_2	5	weighting scalar β	4×10^4	weighting scalar α	100

Eq. (4). To robustly track the planned CoM manifolds, we minimize a finite-phase quadratic cost function and solve for the continuous control parameters as follows

$$\begin{aligned} &\min_{\boldsymbol{u}_{\boldsymbol{x}}^c} \ \mathcal{V}_N(q,\ \boldsymbol{x}_N) + \sum_{n=0}^{N-1} \eta^n \mathcal{L}_n(q, \boldsymbol{x}_n, \boldsymbol{u}_{\boldsymbol{x}}^c) \\ &\text{subject to}: \ \dot{\boldsymbol{x}} = \boldsymbol{\mathcal{F}}_{\boldsymbol{x}}(\boldsymbol{x}, \boldsymbol{u}_{\boldsymbol{x}}^c, d), \\ &\qquad\qquad \omega^{\min} \le \omega \le \omega^{\max}, \tau_y^{\min} \le \tau_y \le \tau_y^{\max}, \end{aligned} \tag{13}$$

where $\boldsymbol{u}_{\boldsymbol{x}}^c = \{\omega, \tau_y\}$ corresponds to the continuous variables of the hybrid control input $\boldsymbol{u}_{\boldsymbol{x}}$, ω defined in Eq. (5) is equivalent to modulating the ground reaction force, $0 \le \eta \le 1$ is a discount factor, N is the number of discretized stages until the next step transition[3], ζ_{trans}, the terminal cost is $\mathcal{V}_N = \alpha(\dot{x}(\zeta_{\text{trans}}) - \dot{x}(\zeta_{\text{trans}})^{\text{des}})^2$. Here, $\dot{x}(\zeta_{\text{trans}})$ is the final velocity at the instant of the next step transition and $\dot{x}(\zeta_{\text{trans}})^{\text{des}}$ is the desired nominal velocity at the transition instant. The first constraint $\boldsymbol{\mathcal{F}}_{\boldsymbol{x}}(\cdot)$ is defined by the sagittal PIPM dynamics of Eq. (4) with an extra input disturbance d. Additionally, $\mathcal{L}_n$ is the one step cost-to-go function at the n^{th} stage defined as a weighted square sum of the tracking errors and control variables:

$$\mathcal{L}_n = \int_{\zeta_{q,n}}^{\zeta_{q,n+1}} [\beta\sigma^2 + \Gamma_1\tau_y^2 + \Gamma_2(\omega - \omega^{\text{ref}})^2] d\zeta,$$

where, σ is the phase-space manifold of Section III-D used as a feedback control parameter, $\zeta_{q,n}$ and $\zeta_{q,n+1}$ are the starting and ending phase progression values at the n^{th} and $(n+1)^{\text{th}}$ stage for the q^{th} walking step, α, β, Γ_1 and Γ_2 are weights, and ω^{ref} is the reference phase-space asymptote slope. This algorithm generates optimal control policies, which imply bounded values for ω and τ_y. It does not consider flywheel position limits at this moment as our focus has been on outlining a proof-of-concept control approach. To implement this type of controller in the future, we will need to account for the flywheel dynamics and the constraint on its position.

To avoid chattering effects[4] in the neighborhood of the planned manifold, a ϵ-boundary layer is defined and used to saturate the controls, i.e.

$$\boldsymbol{u}_{\boldsymbol{x}}^{c'} = \begin{cases} \boldsymbol{u}_{\boldsymbol{x}}^c & |\sigma| > \epsilon \qquad (14a) \\ \dfrac{|\sigma|}{\epsilon}\boldsymbol{u}_{\boldsymbol{x}}^{c,\epsilon} + \dfrac{\epsilon - |\sigma|}{\epsilon}\boldsymbol{u}_{\boldsymbol{x}}^{c,\text{ref}} & |\sigma| \le \epsilon \qquad (14b) \end{cases}$$

[3]We use phase-space intersection as the step transition strategy [1].

[4]This chattering is caused by digital controllers with finite sampling rate. In theory, an infinite switching frequency will be required. However, the control input in practice is constant within a sampling interval, and thus, the real switching frequency can not exceed the sampling frequency. This limitation leads to the chattering.

where ϵ corresponds to the boundary value of an invariant bundle $\mathcal{B}(\epsilon)$ as defined in Def. 1, $\boldsymbol{u}_{\boldsymbol{x}}^{c,\epsilon} = \{\omega^\epsilon, \tau_y^\epsilon\}$ are control inputs at the instant when the trajectory enters the invariant bundle $\mathcal{B}(\epsilon)$, $\boldsymbol{u}_{\boldsymbol{x}}^{c,\text{ref}} = \{\omega^{\text{ref}}, \tau_y^{\text{ref}}\}$ are nominal control inputs. The smoothness of the above controller is studied in [44]. As Eq. (14) shows, when $|\sigma| \le \epsilon$, the control effort, $\boldsymbol{u}_{\boldsymbol{x}}^{c'}$ is scaled between $\boldsymbol{u}_{\boldsymbol{x}}^{c,\epsilon}$ and $\boldsymbol{u}_{\boldsymbol{x}}^{c,\text{ref}}$. This control law is composed of an "inner" and an "outer" controller. The "outer" controller steers states into $\mathcal{B}(\epsilon)$ while the "inner" controller maintains states within $\mathcal{B}(\epsilon)$. Recovery trajectories are shown in Fig. 5 for two scenarios in the presence of random disturbances.

Since the control is bounded, we need to define a new control-dependent recoverability bundle. Given an acceptable deviation ϵ_0 from the manifold, the invariant bundle is $\mathcal{B}(\epsilon_0)$. The control policy of Eq. (14) generates a control-dependent recoverability bundle (a.k.a., region of attraction to the "boundary-layer") defined as $\mathcal{R}(\epsilon, \zeta_{\text{trans}}) = \big\{\boldsymbol{x}_\zeta \in \mathbb{R}^2,\ \zeta_0 \le \zeta \le \zeta_{\text{trans}} \ \big|\ \boldsymbol{x}_{\zeta_{\text{trans}}} \in \mathcal{B}(\epsilon),\ \boldsymbol{u}_{\boldsymbol{x}}^c \in \boldsymbol{u}_{\boldsymbol{x}}^{c,\text{range}}\big\}$, where $\boldsymbol{u}_{\boldsymbol{x}}^{c,\text{range}}$ are the control bounds shown in Eq. (13).

Theorem (Existence of Recoverability Bundle)**.** *Given the phase progression transition value ζ_{trans} and the control policy of Eq. (14), a recoverability bundle $\mathcal{R}(\epsilon, \zeta_{\text{trans}})$ exists and can be estimated by a maximum tube radius $\sigma_0^{\max}$.*

Proof: Given an initial disturbed state $\sigma_0 > \epsilon$ and assuming the existence of a control policy such that $\sigma_{\text{trans}} \le \epsilon$, then the recoverability bundle $\mathcal{R}(\epsilon, \zeta_{\text{trans}})$ exists. Let us consider a Lyapunov function $V = \sigma^2/2$. Taking the derivative of V along the pendulum dynamics of Eq. (4), we get

$$\begin{aligned} \dot{V} &= \sigma\dot{x}_{\text{apex}}^2\big(-2\dot{x}(x - x_{\text{foot}}) + 2\dot{x}\ddot{x}/\omega^2\big) \\ &= \sigma\dot{x}_{\text{apex}}^2\Big(-2\dot{x}(x - x_{\text{foot}}) + 2\dot{x}\big((x - x_{\text{foot}}) - \frac{\tau_y}{mg}\big)\Big) \\ &= -\frac{2\dot{x}_{\text{apex}}^2\sigma\dot{x}\tau_y}{mg} = -\frac{2\sqrt{2}\dot{x}_{\text{apex}}^2\dot{x}\tau_y \cdot \text{sign}(\sigma)}{mg}\sqrt{V} \le 0. \end{aligned}$$

which can be used to prove the stability (i.e., attractiveness) of $\sigma = 0$. For example, consider the case of forward walking, $\dot{x} > 0$. Then, as long as $\sigma \cdot \tau_y > 0$, i.e., the pitch torque has the same sign as σ, the attractiveness is guaranteed. That is, if $\sigma > 0$ (the robot moves forward faster than expected), then we need $\tau_y > 0$ to slow down, and vice-versa. If $\tau_y = 0$, then $\dot{V} = 0$, which implies a zero convergence rate. This means that the CoM state will follow its natural inverted pendulum dynamics without converging. As such, in order to converge to the desired invariant bundle, control action τ_y is required. To estimate $\mathcal{R}(\epsilon, \zeta_{\text{trans}})$, we use the optimal control policy proposed in Eq. (14). Assuming $\sigma \cdot \tau_y > 0$ (i.e., $\tau_y \cdot \text{sign}(\sigma) =$

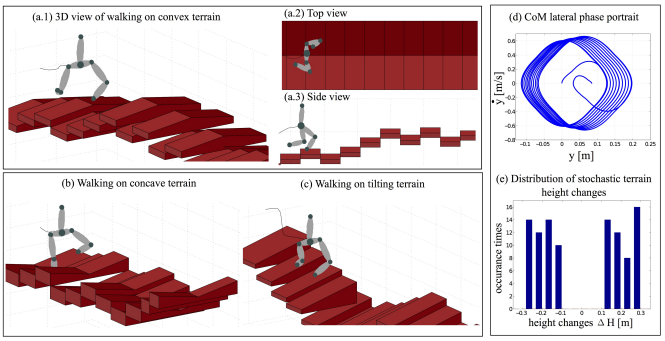

Fig. 6: Traversing various rough terrains. The subfigures on the left block show dynamic locomotion over rough terrains with varying heights. The block on the right shows the lateral phase-space trajectory and height variation distribution over 100-steps.

$|\tau_y|$) and a minimum torque action is applied, i.e., $|\tau_y| > |\tau_y^{\min}|$, the equation above becomes

$$\dot{V} < -\frac{2\sqrt{2}\dot{x}_{\text{apex}}^2 \dot{x}|\tau_y^{\min}|}{mg}\sqrt{V} < 0. \tag{15}$$

The bounded $\dot{V}$ above can be integrated from the initial state to the next transition instant

$$\int_{V_0}^{V_{\text{trans}}} \frac{dV}{\sqrt{V}} < -\int_{t_0}^{t_{\text{trans}}} \mu\dot{x}|\tau_y^{\min}|dt = -\mu|\tau_y^{\min}|(x_{\text{trans}} - x_0),$$

where $\mu = (2\sqrt{2}\dot{x}_{\text{apex}}^2)/(mg)$. The equation above can be developed to $\sqrt{V_0} < \sqrt{V_{\text{trans}}} + \mu \cdot (x_{\text{trans}} - x_0) \cdot |\tau_y^{\min}|/2$. Since $V_0 = \sigma_0^2/2, V_{\text{trans}} = \sigma_{\text{trans}}^2/2 \leq \epsilon^2/2$, we have

$$\sigma_0 < \epsilon + \frac{\sqrt{2}}{2}\mu \cdot (x_{\text{trans}} - x_0) \cdot |\tau_y^{\min}| = \sigma_0^{\max}.$$

where $\sigma_0^{\max}$ defines the maximum tube radius at the initial instant from which the robot can recover from. Therefore we can re-write the recoverability bundle of Def. 2 as:

$$\mathcal{R}(\epsilon, \zeta_{\text{trans}}) = \left\{ \boldsymbol{x}_\zeta \in \mathbb{R}^2,\ \zeta_0 \leq \zeta \leq \zeta_{\text{trans}} \mid \sigma_0 \leq \sigma_0^{\max} \right\}.$$

The existence of a recoverability bundle has been proven with a maximum tube radius. ■

Remark 3. *Our algorithm is applicable to forward, backward walking or forward-to-backward transitions just by planning the proper sequence of apex states.*

B. Second-stage: Discrete Foot Placement Control

When a disturbance is large enough to bring the CoM state outside its recoverability bundle $\mathcal{R}(\epsilon, \zeta_{\text{trans}})$, the controller can not recover to the invariant bundle. Let us consider planning the next transition step to occur when the CoM is at the same position than it was originally planned for. We also assume that we keep the previously planned apex velocity $\dot{x}_{\text{apex},q_{k+1}}$ for the next step. We can solve for a new foot placement by using the analytical solution of Section III-D. Let us consider the disturbed phase-space transition state, $(x_{\text{trans}}, \dot{x}_{\text{trans}}^{\text{dist}})$. Using Eq. (12), we get

$$x_{\text{foot},q_{k+1}} := x_{\text{trans}} + \frac{1}{\omega}(\dot{x}_{\text{trans}}^{\text{dist}2} - \dot{x}_{\text{apex},q_{k+1}}^2)^{1/2}. \tag{16}$$

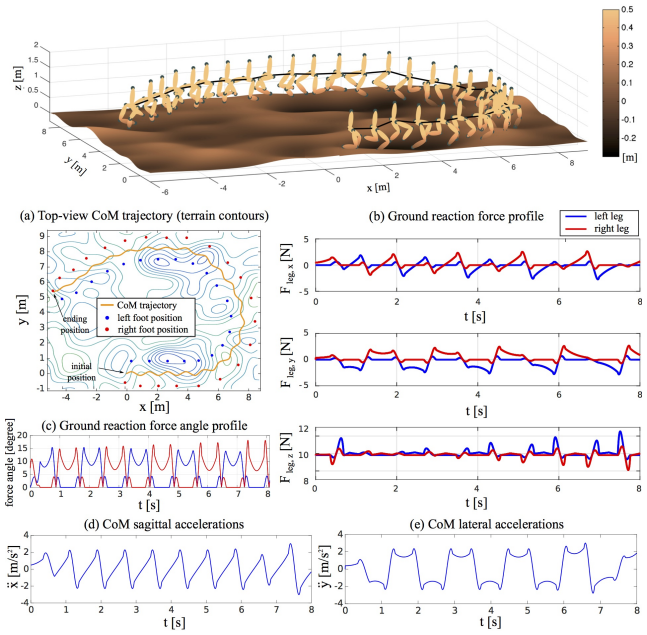

Fig. 7: Circular walking over random rough terrain. The 3D figure above shows dynamic walking while steering. The terrain height randomly varies within $[-0.24, 0.3]$ m. Subfigure (a) shows the top view of the CoM trajectory and the foot locations given the terrain contour. (b) shows each leg's ground reaction forces in local coordinate. The reaction forces at step transitions are smooth thanks to the multi-contact control phase. (c) shows the angle of reaction forces is constrained within the 45° friction cone. (d) and (e) show smooth CoM sagittal and lateral accelerations.

For forward walking, $x_{\text{foot},q_{k+1}} > x_{\text{trans}}$, so we ignore the solution with the negative square root. Note that if $\dot{x}_{\text{apex}_{q+1}} = 0$, i.e., coming to a stop, Eq. (16) becomes $x_{\text{foot}_{q+1}}^{\text{rep}} = x_{\text{trans}} + \dot{x}_{\text{trans}}^{\text{dist}}/\omega$. In such case, this equation is the same as the Capture Point dynamics in [45].

Once this sagittal foot placement is re-computed, a lateral foot position is also planned using a searching strategy [1]. To conclude, this two-stage procedure defines our robust optimal phase-space planning strategy[5].

V. Dynamic Maneuvering over Various Terrains

In this section, our hybrid phase-space planning and robust optimal controller is tested over various terrains and subject to external disturbances. Inverse kinematics are used to map three-dimensional CoM and foot positions to joint angles. An accompanying video of the dynamic walking over various terrains is available at https://youtu.be/F8uTHsqn1dc.

Example 2 (Dynamic Walking over Rough Terrains)**.** *Three challenging terrains with random but known height variations are tested as shown in Fig. 6: (a) a terrain with convex steps, (b) a terrain with concave steps and (c) a terrain with inclined steps. The height variation, Δh_k, of two consecutive steps is randomly generated based on the uniform distribution,*

$$\Delta h_k \sim \text{Uniform}\left\{(-\Delta h_{\max}, -\Delta h_{\min}) \cup (\Delta h_{\min}, \Delta h_{\max})\right\},$$

[5]Our recovery strategies are computationally efficient: (i) Once disturbance is applied, an optimal policy is obtained by quickly searching a previously generated offline policy table. (ii) If the trajectory cannot recover before ζ_{trans}, a new foot placement is re-planned using Eq. (16). Relying on an analytical foot placement strategy allows to speed up computation.

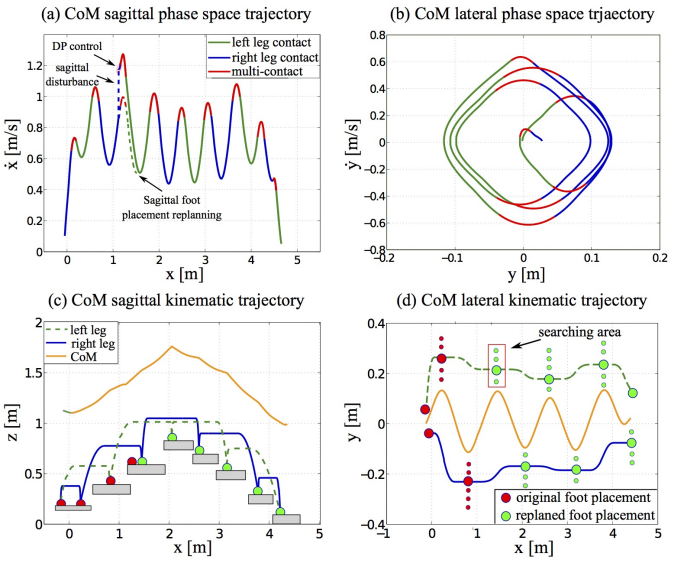

Fig. 8: Rough terrain recovery from sagittal disturbance by hybrid control strategy. The planner uses both first-stage DP for continuous control and second-stage discrete foot placement re-planning to recover from a CoM sagittal push. As subfigures (a) and (b) show, a multi-contact transition is used in this walking. Subfigures (c) and (d) show the sagittal and lateral kinematic CoM and foot trajectories.

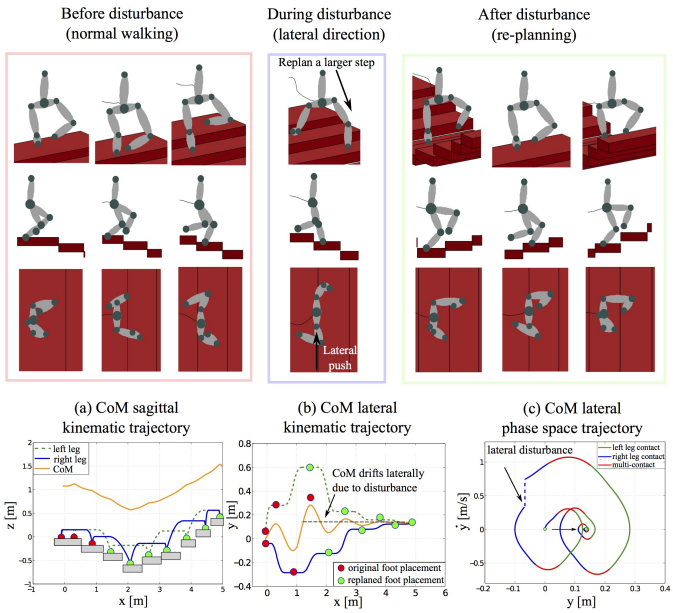

Fig. 9: Rough terrain dynamic walking under lateral disturbance. During the lateral disturbance phase, the robot re-plans its foot placement to achieve balanced walking.

where $\Delta h_{\min} = 0.1$ *m,* $\Delta h_{\max} = 0.3$ *m. A* 10° *tilt angle is used for the slope of the steps. Foot placements are chosen a priori using simple kinematic rules. We design apex velocities according to a heuristic accounting for terrain heights, and we use an average apex velocity of* 0.6 *m/s. Finally we design piecewise linear CoM surfaces that conform to the terrain. We then apply the proposed planning pipeline to generate trajectories and search step transitions. The lateral CoM phase portrait in Fig. 6 (d) shows stable walking over 25 steps. The bar graph in Fig. 6 (e) shows the distribution of the randomly generated terrain heights over 100 steps.*

Example 3 (Circular Walking over Random Rough Terrain)**.** *Circular walking over random rough terrain is shown in Fig. 7. We use this example to validate the steering capability of our planner. The walking direction is defined by the heading angle* θ *shown in Def. 4. The planning process is performed in the robot's local coordinate with respect to the heading angle. We then apply a local-to-global transformation.*

Example 4 (Recovery from Sagittal Disturbance)**.** *A sagittal push is applied to the robot as shown in Fig. 8 (a). This disturbance is considerably large such that the phase-space state can not recover to its nominal PSM before the next step transition. Thus, a sagittal foot placement needs to be re-planned as previously explained. The dashed line of Fig. 8 (a) represents the original phase-space trajectory while the solid line represents the re-planned trajectory.*

Example 5 (Recovery from Lateral Disturbance)**.** *At the third step, the robot receives a lateral CoM disturbance, which causes a CoM lateral drift shown in Fig. 9 (b) and a lateral velocity jump shown in Fig. 9 (c). To deal with this disturbance, a new lateral foot placement is re-planned while ensuring that a lateral quasi-limit cycle is maintained.*

VI. CONCLUSIONS

The main focus of this paper has been on addressing the needs for robust planning and control of non-periodic bipedal locomotion behaviors. These types of behaviors arise in situations where terrains are highly irregular. Many bipedal locomotion frameworks have been historically focused on flat terrain or mildly rough terrain locomotion behaviors. An increasing number of them are making their way into planning locomotion over rougher or inclined terrains. In contrast, our effort is centered around the goals of (i) providing metrics of robustness in rough terrain for robust control of the locomotion behaviors, (ii) generalizing gaits to any types of terrain topologies, (iii) providing formal tools to study planning, robustness, and recoverability of the non-periodic gaits, and (iv) demonstrating the ability of our framework to deal with large external disturbances. Our future work will focus on: (i) experimental validations of the proposed optimal control strategy, where pose estimation and kinematic errors, among other problems, will greatly impact the real performance; (ii) a realistic terrain perception model that does not assume perfect terrain information; (iii) a more realistic robot model that incorporates swing leg dynamics.

ACKNOWLEDGMENTS

This work was supported by the Office of Naval Research, ONR Grant [grant #N000141210663], NASA Johnson Space Center, NSF/NASA NRI Grant [grant #NNX12AM03G], and NSF CPS Synergy Grant [grant #1239136]. We would like to express our special thanks to Steven Jens Jorgensen for his helpful suggestions and review. We are also grateful to other HCRL members for their valuable discussions.

REFERENCES

[1] Ye Zhao and Luis Sentis. A three dimensional foot placement planner for locomotion in very rough terrains. In *IEEE-RAS International Conference on Humanoid Robots, 2012*, pages 726–733, 2012.

[2] Jia-chi Wu and Zoran Popović. Terrain-adaptive bipedal locomotion control. In *ACM Transactions on Graphics*, volume 29, page 72. ACM, 2010.

[3] Tomomichi Sugihara. Dynamics morphing from regulator to oscillator on bipedal control. In *IEEE/RSJ International Conference on Intelligent Robots and Systems*, pages 2940–2945, 2009.

[4] Ko Yamamoto and Takuya Shitaka. Maximal output admissible set for limit cycle controller of humanoid robot. In *IEEE-RAS International Conference on Robotics and Automation*, pages 5690–5697, 2015.

[5] Camille Brasseur, Alexander Sherikov, Cyrille Collette, Dimitar Dimitrov, and Pierre-Brice Wieber. A robust linear mpc approach to online generation of 3d biped walking motion. In *IEEE-RAS International Conference on Humanoid Robots*, pages 595–601, 2015.

[6] Hui-Hua Zhao, Wen-Loong Ma, Michael B Zeagler, and Aaron D Ames. Human-inspired multi-contact locomotion with amber2. In *ICCPS'14: ACM/IEEE 5th International Conference on Cyber-Physical Systems*, pages 199–210, 2014.

[7] Quan Nguyen and Koushil Sreenath. Optimal robust control for bipedal robots through control lyapunov function based quadratic programs. In *Robotics: Science and Systems*, 2015.

[8] Marc H Raibert. *Legged robots that balance*. MIT press, 1986.

[9] Jerry Pratt, Chee-Meng Chew, Ann Torres, Peter Dilworth, and Gill Pratt. Virtual model control: An intuitive approach for bipedal locomotion. *The International Journal of Robotics Research*, 20(2):129–143, 2001.

[10] Jessy W Grizzle, Christine Chevallereau, Ryan W Sinnet, and Aaron D Ames. Models, feedback control, and open problems of 3d bipedal robotic walking. *Automatica*, 50(8):1955–1988, 2014.

[11] Alireza Ramezani, Jonathan W Hurst, Kaveh Akbari Hamed, and JW Grizzle. Performance analysis and feedback control of atrias, a three-dimensional bipedal robot. *Journal of Dynamic Systems, Measurement, and Control*, 136(2):021012, 2014.

[12] Eric R Westervelt, Jessy W Grizzle, Christine Chevallereau, Jun Ho Choi, and Benjamin Morris. *Feedback control of dynamic bipedal robot locomotion*, volume 28. CRC press, 2007.

[13] T Yang, ER Westervelt, A Serrani, and James P Schmiedeler. A framework for the control of stable aperiodic walking in underactuated planar bipeds. *Autonomous Robots*, 27(3):277–290, 2009.

[14] Jerry Pratt, John Carff, Sergey Drakunov, and Ambarish Goswami. Capture point: A step toward humanoid push recovery. In *IEEE-RAS International Conference on Humanoid Robots*, pages 200–207, 2006.

[15] Toru Takenaka, Takashi Matsumoto, and Takahide Yoshiike. Real time motion generation and control for biped robot-1st report: Walking gait pattern generation. In *IEEE/RSJ International Conference on Intelligent Robots and Systems*, pages 1084–1091, 2009.

[16] At L Hof. The 'extrapolated center of mass' concept suggests a simple control of balance in walking. *Human Movement Science*, 27(1):112–125, 2008.

[17] Johannes Englsberger, Christian Ott, and Alin Albu-Schaffer. Three-dimensional bipedal walking control based on divergent component of motion. *IEEE Transactions on Robotics*, 31(2): 355–368, 2015.

[18] Mitsuharu Morisawa, Shuuji Kajita, Fumio Kanehiro, Kenji Kaneko, Kanako Miura, and Kazuhito Yokoi. Balance control based on capture point error compensation for biped walking on uneven terrain. In *IEEE-RAS International Conference on Humanoid Robots*, pages 734–740, 2012.

[19] Oscar E Ramos and Kris Hauser. Generalizations of the capture point to nonlinear center of mass paths and uneven terrain. In *IEEE-RAS International Conference on Humanoid Robots*, pages 851–858, 2015.

[20] Yiping Liu, Patrick M Wensing, David E Orin, and Yuan F Zheng. Trajectory generation for dynamic walking in a humanoid over uneven terrain using a 3d-actuated dual-slip model. In *IEEE/RSJ International Conference on Intelligent Robots and Systems*, pages 374–380, 2015.

[21] Scott Kuindersma, Robin Deits, Maurice Fallon, Andrés Valenzuela, Hongkai Dai, Frank Permenter, Twan Koolen, Pat Marion, and Russ Tedrake. Optimization-based locomotion planning, estimation, and control design for the atlas humanoid robot. *Autonomous Robots*, pages 1–27, 2015.

[22] Siyuan Feng, Eric Whitman, X Xinjilefu, and Christopher G Atkeson. Optimization-based full body control for the darpa robotics challenge. *Journal of Field Robotics*, 32(2):293–312, 2015.

[23] Hongkai Dai and Russ Tedrake. Optimizing robust limit cycles for legged locomotion on unknown terrain. In *IEEE Conference on Control and Decision*, pages 1207–1213, 2012.

[24] Katie Byl and Russ Tedrake. Metastable walking machines. *The International Journal of Robotics Research*, 28(8):1040–1064, 2009.

[25] Ian R Manchester, Uwe Mettin, Fumiya Iida, and Russ Tedrake. Stable dynamic walking over uneven terrain. *The International Journal of Robotics Research*, 30(3):265–279, 2011.

[26] Ian R Manchester and Jack Umenberger. Real-time planning with primitives for dynamic walking over uneven terrain. In *IEEE International Conference on Robotics and Automation*, pages 4639–4646, 2014.

[27] Andreas Hofmann. *Robust execution of bipedal walking tasks from biomechanical principles*. PhD thesis, Massachusetts Institute of Technology, 2006.

[28] Zhibin Li, Chengxu Zhou, Juan Castano, Xin Wang, Francesca Negrello, Nikos G Tsagarakis, and Darwin G Caldwell. Fall prediction of legged robots based on energy state and its implication of balance augmentation: A study on the humanoid. In *IEEE-RAS International Conference on Robotics and Automation*, pages 5094–5100, 2015.

[29] Benjamin Stephens. Humanoid push recovery. In *IEEE-RAS International Conference on Humanoid Robots*, pages 589–595, 2007.

[30] S Hyon and Gordon Cheng. Disturbance rejection for biped humanoids. In *IEEE-RAS International Conference on Robotics and Automation*, pages 2668–2675, 2007.

[31] Taku Komura, Howard Leung, Shunsuke Kudoh, and James Kuffner. A feedback controller for biped humanoids that can counteract large perturbations during gait. In *IEEE-RAS International Conference on Robotics and Automation*, pages 1989–1995, 2005.

[32] Steven M LaValle. Planning algorithms. In *Cambridge university press*, 2006.

[33] Shuuji Kajita and Kazuo Tan. Study of dynamic biped locomotion on rugged terrain-derivation and application of the linear inverted pendulum mode. In *IEEE-RAS International Conference on Robotics and Automation*, pages 1405–1411, 1991.

[34] Igor Mordatch, Martin De Lasa, and Aaron Hertzmann. Robust physics-based locomotion using low-dimensional planning. *ACM Transactions on Graphics*, 29(4):71, 2010.

[35] Manoj Srinivasan and Andy Ruina. Computer optimization of a minimal biped model discovers walking and running. *Nature*,

439(7072):72–75, 2006.

[36] Ye Zhao, Jonathan Samir Matthis, Sean L. Barton, Mary Hayhoe, and Luis Sentis. Exploring visually guided locomotion over complex terrain: A phase-space planning method. In *Dynamic Walking Conference*, 2016.

[37] Johannes Englsberger, Twan Koolen, Sylvain Bertrand, Jerry Pratt, Christian Ott, and Alin Albu-Schaffer. Trajectory generation for continuous leg forces during double support and heel-to-toe shift based on divergent component of motion. In *IEEE/RSJ International Conference on Intelligent Robots and Systems*, pages 4022–4029, 2014.

[38] Michael S Branicky, Vivek S Borkar, and Sanjoy K Mitter. A unified framework for hybrid control: Model and optimal control theory. *IEEE Transactions Automatic Control*, 43(1): 31–45, 1998.

[39] Emilio Frazzoli. *Robust hybrid control for autonomous vehicle motion planning*. PhD thesis, Massachusetts Institute of Technology, 2001.

[40] Ye Zhao, Ufuk Topcu, and Luis Sentis. Towards formal planner synthesis for unified legged and armed locomotion in constrained environments. In *Dynamic Walking Conference*, 2016.

[41] Ye Zhao, Ufuk Topcu, and Luis Sentis. High-level reactive planner synthesis for unified legged and armed locomotion in constrained environments. In *IEEE Conference on Decision and Control, Under Review*, 2016.

[42] Ye Zhao, Donghyun Kim, Benito Fernandez, and Luis Sentis. Phase space planning and robust control for data-driven locomotion behaviors. In *IEEE-RAS International Conference on Humanoid Robots*, 2013.

[43] Ye Zhao. *Phase Space Planning for Robust Locomotion*. Master thesis, The University of Texas at Austin, 2013.

[44] Vadim I Utkin. *Sliding modes in control and optimization*. Springer Science & Business Media, 2013.

[45] Johannes Engelsberger, Christian Ott, Mximo A. Roa, Alin Albu-Schaffer, and Gerhard Hirzinger. Bipedal walking control based on capture point dynamics. In *IEEE/RSJ International Conference on Intelligent Robots and Systems*, pages 4420–4427, 2011.